ACSNANO

www.acsnano.org

ARTICLE

Highly Tumor-Specific and Long-Acting Iodine-131 Microbeads for Enhanced Treatment of Hepatocellular Carcinoma with Low-Dose Radio-Chemoembolization

Yuyi Qian,[⊥] Qiufang Liu,[⊥] Panli Li,[⊥] Yaobao Han,[⊥] Jianping Zhang, Jiaojiao Xu, Jingwen Sun, Aihua Wu, Shaoli Song,* and Wei Lu*

Cite This: https://dx.doi.org/10.1021/acsnano.0c09122

Read Online

ACCESS | Metrics & More | Article Recommendations | Supporting Information

ABSTRACT: Transarterial radioembolization (TARE) is considered the standard treatment for intermediate-stage hepatocellular carcinoma (HCC). Iodine-131 (^{131}I)-labeled lipiodol TARE is an effective treatment for HCC but has been withdrawn due to its poor retention in tumor lesions and significant distribution in normal tissues with severe side effects. In this work, a highly tumor-specific ^{131}I-TARE agent with long-time retention is developed by simply introducing tyrosine to poly(vinyl alcohol) (PVA) drug-eluting microbeads (Tyr-PVA-DEBs). The labeling efficiency of ^{131}I-labeled microbeads remains above 85% in 50% serum for 31 days. Micro-single-photon emission computed tomography/computed tomography (μSPECT/CT) evidences that the ^{131}I-labeled microbeads accumulate in the orthotopic N1S1 hepatoma of rats for 31 days following intra-arterial injection. The cumulative radiation dose per cubic centimeter of the tumor is at least 13 678-fold higher than that of normal tissues. The highly tumor-selective radiation of the ^{131}I-labeled microbeads allows localized delivery of 345.04 ± 139.16 Gy to the tumor following a single injection dose as low as 0.2 mCi of ^{131}I. Moreover, the ^{131}I-labeled microbeads are loaded with doxorubicin hydrochloride (DOX) through the carboxy groups on tyrosine of the polymer. The ^{131}I-DOX-loaded microbeads present a synergetic antitumor effect without recurrence in comparison with the microbeads labeled with ^{131}I or loading DOX alone, attributed to the sensitization of DOX to ^{131}I-induced ionizing radiation damage to DNA under the embolization-induced hypoxia. Our results demonstrate a high tumor retention of ^{131}I-labeled embolic agent for low-dose transarterial radio-chemoembolization (TARCE) with a synergetic therapeutic effect on treating HCC, showing potential for clinical application.

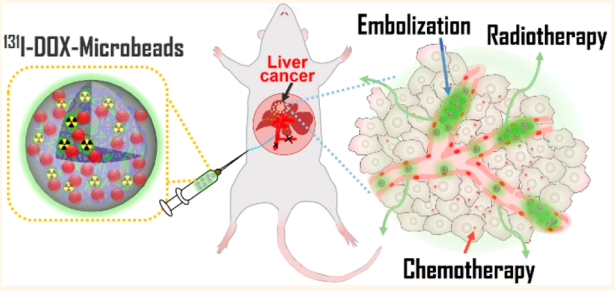

KEYWORDS: *iodine-131, transarterial radioembolization, tumor retention, doxorubicin, hepatocellular carcinoma*

INTRODUCTION

Hepatocellular carcinoma (HCC) is one of the most common and deadliest cancer. Transarterial radioembolization (TARE) is an effective palliative treatment for intermediate−advanced stage HCC that is ineligible for surgery or liver transplantation.[1−3] TARE consisting of yttrium-90 (^{90}Y)-labeled microspheres that deliver high-dose internal radiotherapy to liver tumor has been developed with well-established procedures.[4,5] The commercially available ^{90}Y-labeled microspheres include TheraSphere and SIR-Spheres. The former is a glass microsphere with a particle size of 20−30 μm and a specific activity of 2500 Bq per particle.[4] TheraSphere is the most attractive and effective formulation for HCC treatment, with a response rate of 40−50%.[6] The latter one is a resin microsphere with a particle size of 20−60 μm and a specific activity of 50 Bq per particle.[4] A clinical study has shown that the two types of microspheres exhibit similar therapeutic effects in the treatment of patients with unresectable HCC.[7]

Besides ^{90}Y-labeled microspheres, iodine-131 (^{131}I)- or rhenium-188 (^{188}Re)-labeled lipiodol has been used for TARE therapy of HCC.[8] ^{131}I-labeled lipiodol (^{131}I-lipiodol)

Received: November 1, 2020
Accepted: January 27, 2021

Scheme 1. Schematic illustration of the preparation of ^{131}I-DOX-loaded drug-eluting microbeads (ID-DEBs). The tyrosine-substituted PVA-DEBs (Tyr-PVA-DEBs) are prepared by inverse suspension polymerization using potassium persulfate (KPS) and *N*,*N*,*N*′,*N*′-tetramethylenediamine (TMEDA) as initiator and catalyst, respectively. Tyr-PVA-DEBs are labeled with ^{131}I through the chloramine-T method, followed by loading DOX through ion-exchange to obtain ID-DEBs. PVA-NAAADA, poly(vinyl alcohol)-*N*-acryloyl aminoacetaldehyde dimethyl acetal. NAT, *N*-acryl tyrosine. MBA, *N*,*N*′-methylene bis(acrylamide). I-DEBs, ^{131}I-labeled drug-eluting microbeads. D-DEBs, DOX-loaded drug-eluting microbeads.

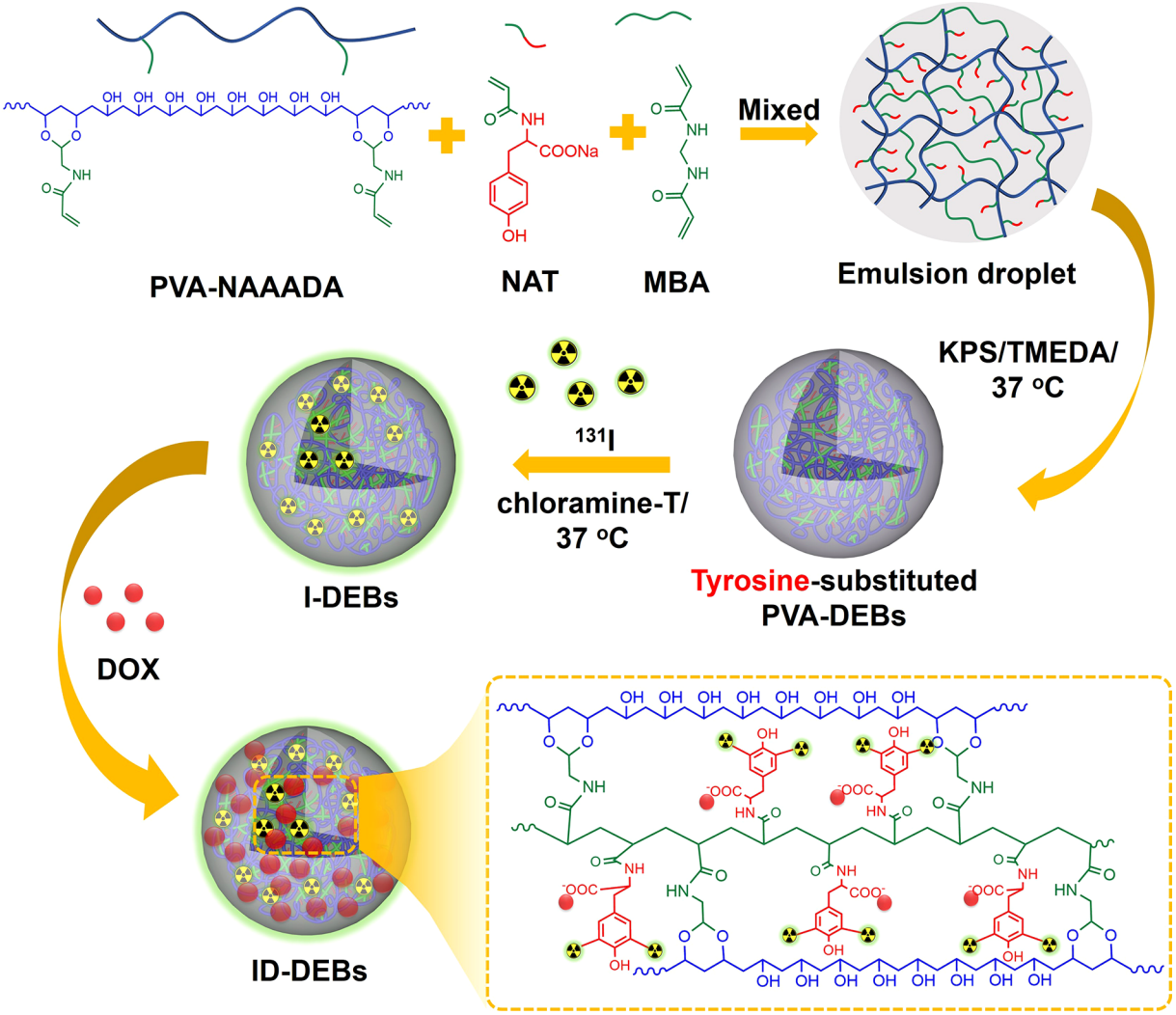

has shown effectiveness in treating patients with HCC and portal vein thrombosis as well as in adjuvant therapy of HCC after surgical resection.[6] Nevertheless, the poor tumor retention of ^{131}I-lipiodol results in its short effective half-life (4.3−5.5 days) in tumor, as well as relatively low tumorous to nontumorous activity ratios following intra-arterial (i.a.) injection.[9,10] Besides, the significant accumulation of ^{131}I-lipiodol in the lung causes adverse effects such as interstitial pneumonia.[11] The systemic distribution of ^{131}I-lipiodol requires the patient to take iodine before the therapy to block thyroid uptake of ^{131}I.[12] Due to the low tumor specificity of ^{131}I-lipiodol, a dose of radioactivity as high as 2.22 GBq (60 mCi) is administrated to the patient to achieve the effective absorbed dose threshold.[6] However, such a dose with high-energetic γ rays emitted by ^{131}I raises concerns about the radioprotective measures.[13] All these limitations owing to the unfavorable embolic characteristic of lipiodol led to the product being withdrawn from the market.[12]

On the other hand, despite the survival benefit in the patients treated with TARE, the therapeutic efficacy remains to be improved to reduce tumor recurrence. Clinical studies have demonstrated a superior overall response and local control rate of patients treated with stereotactic body radiotherapy combined with transarterial chemoembolization (TACE) to that with TACE alone.[14−16] These encouraging outcomes suggest the synergetic effect of the combination of radiotherapy and TACE.[16−18] However, the external radiation induces liver damage, resulting in a total radiation dose limited to 40−60 Gy.[14−16] The advantage of internal radiotherapy with TARE is that it allows delivering a much higher radiation dose to the tumor due to the selectivity.[19,20] To date, there is no multifunctional embolic agent available for transarterial radio-chemoembolization (TARCE) in the clinic.

We have reported poly(lactic-*co*-glycolic acid) (PLGA) embolic microspheres encapsulating hollow CuS nanoparticles and paclitaxel.[21] The microspheres are labeled with ^{131}I through the formation of copper(I) iodide complexes to

https://dx.doi.org/10.1021/acsnano.0c09122
ACS Nano XXXX, XXX, XXX−XXX

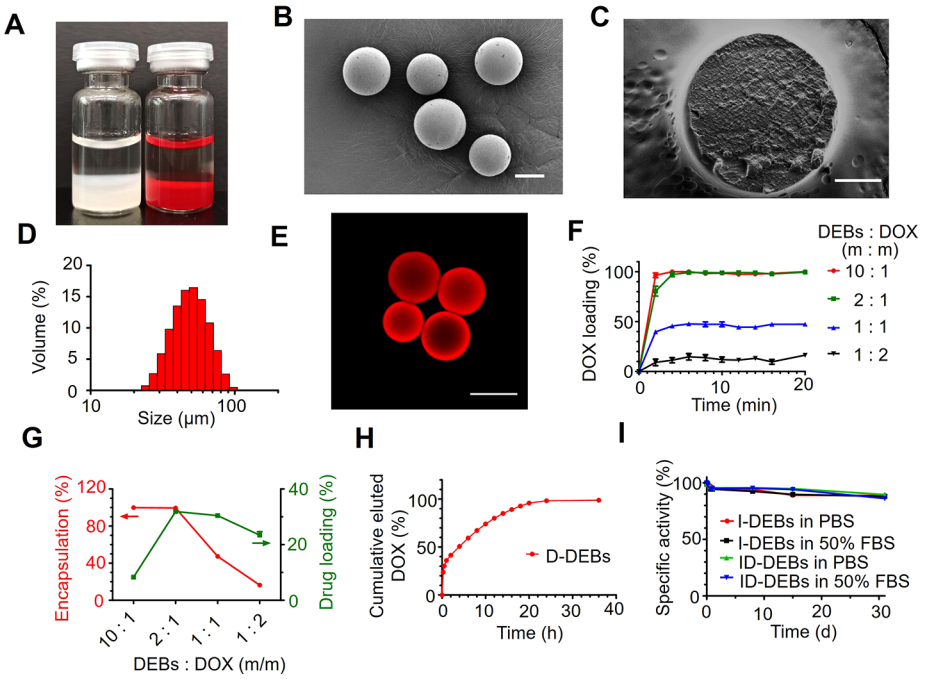

Figure 1. Characterization of ID-DEBs. (A) Photograph of Tyr-PVA-DEBs (left) and DOX-loaded DEBs (D-DEBs, right). (B) Scanning electron micrograph (SEM) of D-DEBs. Bar, 20 μm. (C) SEM of the cross section of D-DEBs. Bar, 10 μm. (D) Size distribution of D-DEBs. (E) Fluorescence micrographs of D-DEBs. Bar, 40 μm. (F) Profiles of DOX loading by D-DEBs over time at different mass ratios of Tyr-PVA-DEBs to DOX. Data are mean ± SD (n = 3). (G) DOX encapsulation (red) or loading (green) efficiency of D-DEBs over different mass ratios of Tyr-PVA-DEBs to DOX. Data are mean ± SD (n = 3). (H) Percentage of the cumulatively eluted DOX from D-DEBs over time in 0.01 M PBS (pH 7.4). Data are mean ± SD (n = 3). (I) Profiles of radiochemical purity of ^{131}I-labeled DEBs (I-DEBs) or ID-DEBs in PBS or 50% FBS over time. FBS, fetal bovine serum. Data are mean ± SD (n = 3).

produce a combinatorial effect of embolization, chemotherapy, radiotherapy, and photothermal therapy on rats bearing tumor transplanted in the liver. However, the ^{131}I-labeling efficiency of the microspheres in serum drops to ~70.2% after 48 h with a low tumor-to-liver activity ratio following i.a. injection, indicating that the ^{131}I-labeling approach remains to be improved.[21]

In this work, we hypothesize that slowly degrading or nondegradable multifunctional embolic agents with stable ^{131}I-labeling offer highly tumor-specific and long-acting TARCE to produce a synergetic antitumor effect on HCC at low dose. To prove this hypothesis, we adopt the design of the clinically applied poly(vinyl alcohol) drug-eluting microbeads (PVA-DEBs) and replace the sulfonate with tyrosine on the polymer (Scheme 1). The tyrosine-substituted PVA-DEBs (Tyr-PVA-DEBs) are labeled with ^{131}I through a simple chloramine-T oxidation method.[22] The ^{131}I-labeled Tyr-PVA-DEBs (I-DEBs) are further loaded with doxorubicin hydrochloride (DOX) through ion-exchange between the positively charged amines of DOX and the carboxy groups on tyrosine of the polymer. The stable ^{131}I-labeling efficiency of I-DEBs enables a selectively high radiation dose per cubic centimeter of tumor, which is at least 13 678-fold higher than that of normal tissues within 31 d following i.a. administration. The high tumor specificity and long retention of I-DEBs afford localized delivery of 345.04 ± 139.16 Gy to the tumor with a single injection dose as low as 0.2 mCi of ^{131}I. The ^{131}I-DOX-loaded microbeads (ID-DEBs) produce a synergetic tumor inhibition on rats bearing orthotopic N1S1 hepatoma without recurrence. The underlying mechanism is the sensitization of DOX to ^{131}I-induced ionizing radiation damage to DNA under hypoxia by embolization.

RESULTS AND DISCUSSION

Characterization of Microbeads. Prior to the formulation, the PVA-based macromer was synthesized by conjugation of *N*-acryloylaminoacetaldehyde dimethylacetal (NAAADA) to the backbone of PVA (Figures S1 and S2). The Tyr-PVA-DEBs were prepared by inverse suspension polymerization of the macromer with the two monomers *N*-acryl tyrosine (NAT) and *N*,*N*′-methylene bis(acrylamide) (MBA), using potassium persulfate (KPS) and *N*,*N*,*N*′,*N*′-tetramethylenediamine (TMEDA) as initiator and catalyst, respectively (Figures S3 and S4). A few minutes after the addition of a DOX solution to Tyr-PVA-DEBs, the microbeads appeared to be red (Figure 1A). Microphotographs and scanning electron micrographs (SEM) depicted that the DOX-loaded Tyr-PVA-DEBs (D-DEBs) had a spherical shape with an average size of 51.4 ± 3.3 μm analyzed by particle size analyzer (Figures 1B–D and S5). Confocal laser scanning microscopy confirmed that DOX was absorbed in the microspheres and distributed on the outer layer of the microspheres. With the increase of radial depth, the distribution of DOX gradually reduced (Figure 1E). Further characterization revealed that DOX was quickly absorbed by Tyr-PVA-DEBs within 2–5 min at various ratios of the microbeads to DOX (Figure 1F). The results of encapsulation efficiency and drug loading efficiency of D-DEBs at different mass ratios of Tyr-PVA-DEBs to DOX demonstrated that the maximum drug loading was 31.93 ± 0.99% with almost 100% encapsulation efficiency (Figure 1G). The drug-eluting curve showed that DOX was quickly and completely eluted from Tyr-PVA-DEBs within 24 h by frequent replacement with bulk fresh medium (Figure 1H), whereas the release of the drug was slow when the volume of sampling and replacement was small

https://dx.doi.org/10.1021/acsnano.0c09122
ACS Nano XXXX, XXX, XXX−XXX

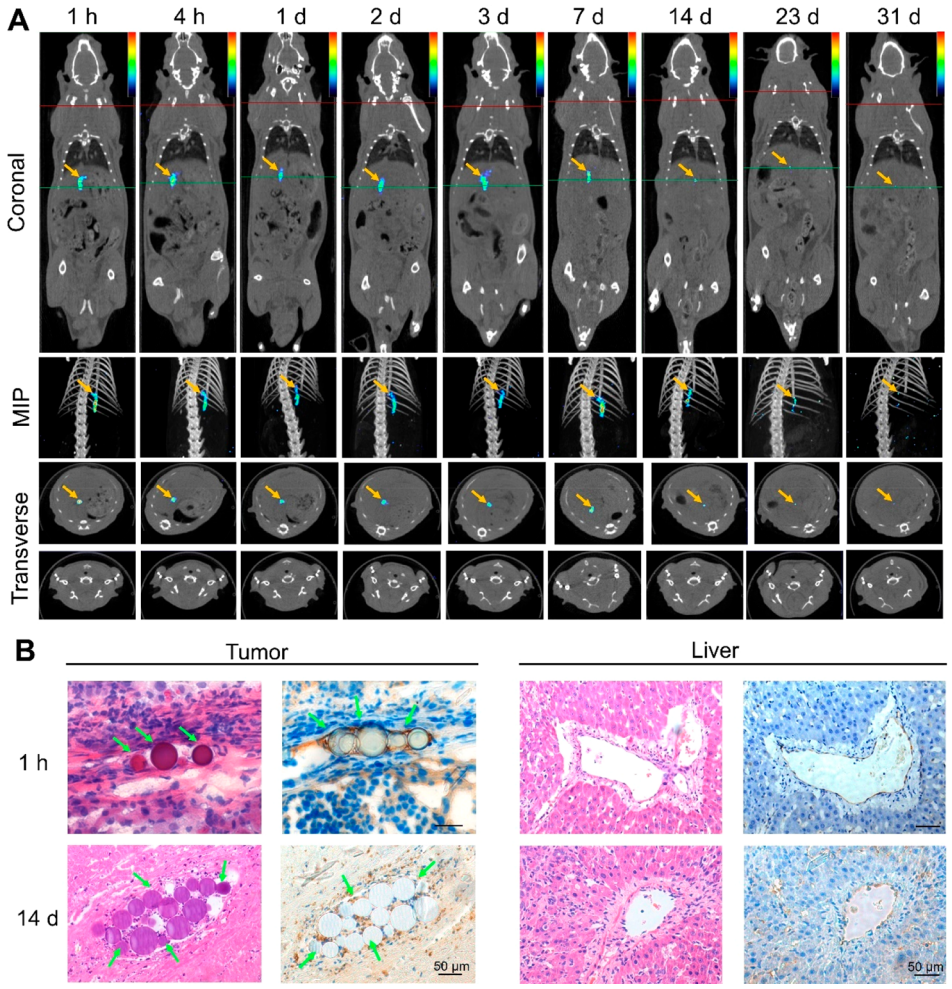

Figure 2. High and specific transarterial embolization of ^{131}I-labeled DEBs (I-DEBs) with long-time tumor retention. (A) Representative μSPECT/CT imaging of I-DEBs in rats bearing orthotopic N1S1 liver tumor at different times following i.a. injection. Arrows, the distribution of I-DEBs in the tumor. Top row, coronal plane of the images. Second row, maximum intensity projection (MIP). Third row, images of the transverse section along the green line across the tumor in the coronal views of the top row. Bottom row, images of the transverse section along the red line across the thyroid in the coronal views of the top row. The scales of the SPECT images at each time point are individually adjusted. (B) H&E staining (left) or CD 31 immunostaining (right) of the tumor or adjacent liver of tumor-bearing rats at 1 h or 14 d following transarterial embolization of I-DEBs. Brown, blood vessels immunostained with anti-CD31 antibody. Arrows, DEBs.

(Figure S6). In order for the comparison with the clinically used microbeads, PVA-DEBs functionalized with 2-acrylamido-2-methylpropanesulfonate sodium salt (AMPS-PVA-DEBs) were additionally prepared and characterized.[23] The prepared AMPS-PVA-DEBs exhibited a similar particle size, morphology, inner structure, and DOX-eluting characteristics to Tyr-PVA-DEBs, except that AMPS-PVA-DEBs had a higher maximum drug loading (Figure S7). However, 1 mL of wet Tyr-PVA-DEBs was measured to carry 41 mg of DOX, which was higher than the loading dose for the commercial DC beads (37.5 mg DOX/mL beads).[24] This result indicated that the DOX loading efficiency of the tyrosine-functionalized DEBs can meet the clinical dose requirement of DEB-mediated TACE.

Using the chloramine T oxidation method, Tyr-PVA-DEBs were able to be labeled with ^{131}I (Figure S8). The maximum specific activity of I-DEBs was about 1.7 mCi/mg with the specific activity per particle of about 15.5 kBq. The specific activity of wet I-DEBs per milliliter was calculated to be about 212.5 mCi, which was more than 7 times that of the clinically applied ^{131}I-lipiodol (30 mCi/mL).[20] More than 85% of ^{131}I was retained on I-DEBs or ID-DEBs following incubation in either phosphate buffer saline (PBS) or 50% fetal bovine serum (FBS) at 37 °C for 31 d (Figure 1I). These results proved that the ^{131}I-labeling of Tyr-PVA-DEBs with or without DOX loading was very efficient and stable. This property was an essential prerequisite for tumor-specific and long-time TARE.

Highly Tumor-Specific and Long-Time Radiation Following Transarterial Embolization of I-DEBs. The biodistribution of I-DEBs in rats bearing N1S1 orthotopic hepatomas following i.a. administration was monitored by micro-single-photon emission computed tomography/computed tomography (μSPECT/CT) thanks to the emission of γ rays by ^{131}I. The procedure of hepatic artery cannulation for i.a. injection is shown in Figure S9. The imaging results showed that the radioisotope accumulated in the tumor site without a significant amount distributed in the liver, thyroid, or other normal tissues at all times after the injection (Figure 2A, arrows). The retention of the radioactivity of I-DEBs in the tumor region was as long as 31 d. Histological examination by

https://dx.doi.org/10.1021/acsnano.0c09122
ACS Nano XXXX, XXX, XXX−XXX

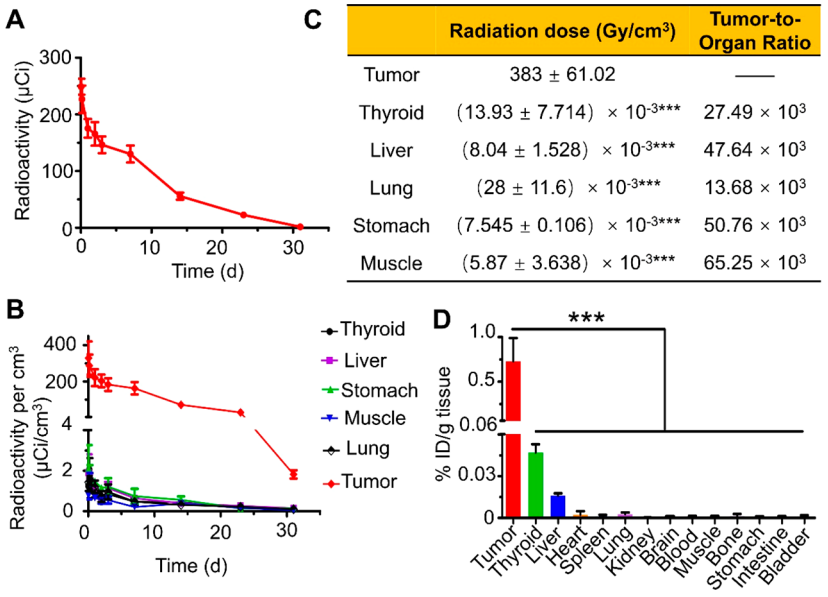

Figure 3. Selectively high radiation dose in tumors following transarterial embolization of I-DEBs at low dose. (A) ^{131}I radioactivity in the tumor of rats bearing N1S1 orthotopic hepatoma over time following i.a. injection of I-DEBs with 0.2 mCi of ^{131}I. Data are presented as mean ± SD (n = 3). (B) ^{131}I radioactivity per cubic centimeter of various normal tissues or tumor over time. Data are presented as mean ± SD (n = 3). (C) Cumulative radiation dose per cubic centimeter of different tissues. Data are presented as mean ± SD (n = 3), calculated from the data in (B). ***p < 0.001 compared to the tumor group analyzed by one-way ANOVA with Tukey's *post hoc* test. (D) Distribution of ^{131}I radioactivity in tumor or different organs at 31 d following administration. % ID/g tissue, percentage injected dose per gram of tissue. Data are presented as mean ± SD (n = 3). ***p < 0.001 compared to the tumor group analyzed by two-way ANOVA with Tukey's *post hoc* test.

hematoxylin and eosin (H&E) staining and CD31 immunostaining confirmed that the i.a. injected microbeads agglomerated to block the blood vessels in the tumor but not the normal liver (Figure 2B). The embolic microbeads remained intact in the tumor for 14 d after the embolization. These results are in line with the stable ^{131}I-labeling property in serum, supporting the highly tumor-specific distribution of I-DEBs with long-time retention.

Strikingly, the cumulative tumor radiation was calculated to be 345.04 ± 139.16 Gy within 31 d following a single i.a. injection of I-DEBs at an ^{131}I dose as low as 0.2 mCi (Figure 3A). The radioactivity per cubic centimeter of tumor was hundreds-fold higher than that of various normal tissues at 23 d postinjection or at the prior time points measured by the μSPECT/CT results (Figure 3B). Compared to the lung, the normal tissue absorbing the highest radiation, the radiation dose per cubic centimeter of the tumor was at least 13 678-fold higher (Figure 3C). The noticeable tumor specificity of radiation was attributed to the accumulation of I-DEBs with high stability of the ^{131}I-labeling. This property enabled the long-time retention of ^{131}I-radiation in the tumor, evidenced by the radioactivity distribution in the tumor at 31 d being 45 times that of the liver, 15 times that of the thyroid, and 264 times that of the lung, respectively (Figure 3D).

Previous dosimetry study showed that the administration dose of ^{131}I-lipiodol limited to 60 mCi per injection in the clinic resulted in the cumulative tumor absorbed radiation dose of 248 ± 176 Gy and indicated the effective tumor-responsive absorbed dose threshold of 280 Gy.[20] The requirement for the high administration dose of ^{131}I-lipiodol was attributed to the low tumor-to-liver uptake ratio of the radioactivity at 24 h postinjection, ranging between 2.3 and 12.[10] To test this, we prepared ^{131}I-lipiodol with high specific activity of ^{131}I in 50% FBS for the biodistribution study (Figure S10A). Following the i.a. injection of ^{131}I-lipiodol to rats bearing N1S1 orthotopic hepatoma, the radio isotope was not only distributed in the tumor but also significantly trapped in the liver (Figure S10B and C). Besides the tumor and liver, a large amount of ^{131}I was distributed in the lung and thyroid (Figure S10D and E). The cumulative tumor radiation was calculated to be only 1.65 ± 0.59 Gy within 21 d following the i.a. injection of ^{131}I-lipiodol at the ^{131}I dose of 0.2 mCi (Figure S10C). The radioactivity per cubic centimeter of tumor did not show a significant difference compared with that of the liver, lung and thyroid, respectively (Figure S10F). These results supported that the low radiation dose in the tumor following the i.a. injection of the liquid ^{131}I-lipiodol was ascribed to its nonspecific and poor retention in the tumor.

In contrast, a much higher tumor cumulative radiation dose of 345.04 ± 139.16 Gy was achieved by the injection of 0.2 mCi of I-DEBs, which was 209 times that of ^{131}I-lipiodol at the same injection dose. This was attributed to the PVA-DEBs for a "permanent" embolization of tumor blood vessels for a long time.[25] The tumor-to-liver activity ratio of I-DEBs was 45 at 31 d postinjection (Figure 3D). To investigate the reason for such high tumor-specific retention of the microspheres, we prepared AMPS-PVA-DEBs with particle sizes of 50 μm or Tyr-PVA-DEBs with particle sizes of 50 or 10 μm for comparison (Figures S7 and S11). The micrographs of H&E staining depicted that the 50-μm-sized AMPS-PVA-DEBs or Tyr-PVA-DEBs accumulated in the tumor vessels without distribution in the liver following i.a. injection (Figure S12A and B). Comparatively, the 10-μm-sized Tyr-PVA-DEBs were distributed in both the tumor and liver (Figure S12C). These results suggested that the tumor-specific distribution of DEBs after hepatic arterial injection was size-dependent, not caused by the tyrosine groups incorporated. DEBs with smaller particle sizes such as 10 μm may not be large enough to

https://dx.doi.org/10.1021/acsnano.0c09122
ACS Nano XXXX, XXX, XXX−XXX

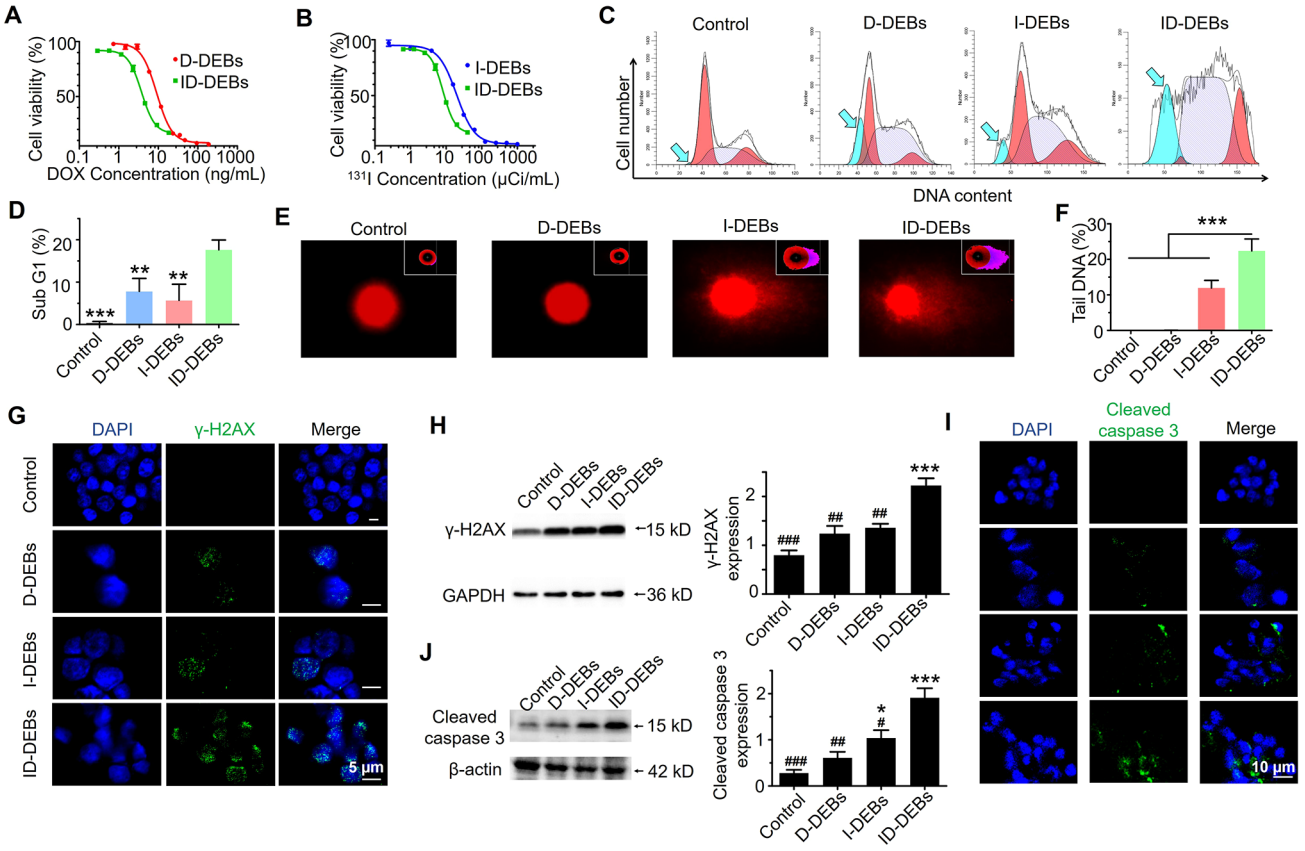

Figure 4. Synergetic antitumor cell effect of ^{131}I and DOX by ID-DEBs under normoxia. (A, B) Cell viability of D-DEBs, I-DEBs or ID-DEBs at various concentrations of DOX (A) or ^{131}I (B) to N1S1 rat hepatoma cells for 72 h determined by the methyl thiazolyl tetrazolium (MTT) assay. Data are presented as mean ± SD (n = 3). (C) Representative cell cycle distribution of N1S1 cells treated with different DEBs. Control, cells without treatment. Arrows, the sub-G1 phase. (D) Percentage of the sub-G1 phase of N1S1 cells following different treatments in (C). Data are represented as mean ± SD (n = 3). **p < 0.01, ***p < 0.001, compared to the ID-DEBs group analyzed by two-way ANOVA with Tukey's *post hoc* test. (E) Representative comet assay images of N1S1 cells with different treatments. Insets, DNA in the tail stained in magenta. (F) Percentages of DNA in the tail by a comet assay in N1S1 cells in (E). Data are represented as mean ± SD (n = 25). ***p < 0.001, compared to the ID-DEBs group analyzed by two-way ANOVA with Tukey's *post hoc* test. (G, H) Representative immunofluorescence micrographs (G) and Western blot and quantitative analysis (H) of γ-H2AX in N1S1 cells following different treatments, respectively. (I, J) Representative immunofluorescence micrographs (I) and Western blot and quantitative analysis (J) of cleaved caspase-3 of N1S1 cells following different treatments, respectively. Cell nuclei were stained with 4′,6-diamidino-2-phenylindole (DAPI). GAPDH or β-actin was used as reference. Data are represented as mean ± SD (n = 3). *p < 0.05, ***p < 0.001 compared to the control group; $^{\#}p$ < 0.05, $^{\#\#}p$ < 0.01, $^{\#\#\#}p$ < 0.001 compared to the ID-DEBs group analyzed by one-way ANOVA with Tukey's *post hoc* test.

completely embolize the tumor blood vessels, resulting in their distribution in the normal liver. The superior embolic property of I-DEBs with an optimal particle size of 50 μm in diameter plus stable ^{131}I-labeling enabled the highly tumor-specific radiation and negligible radiation dose delivered into normal tissues with low toxicity. Besides, the significantly low administration dose applied herein exhibited the potential to reduce the side effects and address the concerns of radioprotective measures brought by the γ radiation from ^{131}I.

In terms of the ^{131}I-labeling procedure, the conventional chloramine-T oxidation method was applied in this study. The free ^{131}I can be removed from the microbeads by centrifugation. The labeling procedure did not require specific equipment and was suitable for operation by nuclear medicine technicians in the hospital. Moreover, like DC beads, I-DEBs were quickly loaded with DOX by a simple mixture right before the transarterial injection without any purification step, feasible for interventional radiologists to operate.

Synergetic Effect of DOX and ^{131}I against N1S1 Rat Hepatoma Cells. Previous research reported a synergetic antitumor effect following co-delivery of DOX and ^{131}I by various nanoparticles following systemic or intratumoral injection.[26−28] As shown in Figures 4A,B and S13, the anti-N1S1 cell effect of DOX from D-DEBs or ^{131}I from I-DEBs was concentration- and time-dependent. At 72 h following incubation, the IC_{50} of DOX from D-DEBs and ^{131}I from I-DEBs was 9.26 ± 0.127 ng/mL and 19.56 ± 1.190 μCi/mL, respectively. The combinatorial treatment of DOX and ^{131}I using ID-DEBs demonstrated an enhanced inhibitory effect, resulting in IC_{50} values of 3.74 ± 0.240 ng/mL of DOX and 8.15 ± 0.521 μCi/mL of ^{131}I, respectively. The combination index (CI) of DOX and ^{131}I from ID-DEBs was calculated to be 0.82. The CI value of less than 1 indicated synergism.[29] Cell cycle arrest and apoptosis are the two modes of action for cell growth inhibition and cell death. To investigate the effect on the cell cycle, the cells were stained with propidium iodide and analyzed by flow cytometry. The tumor cells treated with D-DEBs alone and I-DEBs alone presented 7.83 ± 2.48% and 5.70 ± 3.11% sub-G1 peaks, respectively (Figure 4C and D). Following treatment with ID-DEBs, the sub-G1 cell population

https://dx.doi.org/10.1021/acsnano.0c09122
ACS Nano XXXX, XXX, XXX−XXX

was significantly increased to 17.6 ± 2.31%. The extensive DNA fragmentation occurring in the apoptotic cells following different treatment was detected by single-cell gel electrophoresis. The interrupted DNA strands of the treated cells, after lysis and electrophoresis, migrated out of the nucleus toward the anode, forming a comet tail.[30] As shown in Figure 4E and F, nearly no DNA fragments were observed in the cells of the control group or D-DEBs group, while I-DEBs induced DNA breakage (11.97 ± 2.117%). ID-DEBs (22.39 ± 3.349%) induced almost double the amount of DNA fragments in cells compared with I-DEBs. This result suggested that DOX may prevent the repair from the ionizing radiation-induced DNA damage by altering the abilities of DNA-repair enzymes.[31,32] The damages of double-stranded DNA were confirmed by γ-H2AX staining, showing higher levels of γ-H2AX foci in the ID-DEBs group than that in other groups (Figure 4G and H). The cleavage of caspase 3 is the key event in response to apoptosis. ID-DEBs induced the highest level of cellular cleaved caspase 3 among all the groups (Figure 4I and J). Taken together, these results demonstrated the synergetic tumor cell inhibitory effect of DOX and ^{131}I offered by ID-DEBs, possibly through the mechanism of sensitization of DOX to the radiation-induced DNA damage by ^{131}I.

Enhanced Therapeutic Efficacy of Treating Rats Bearing HCC Following TARCE. Fluorine-18 fluoro-2-deoxyglucose (^{18}F-FDG) micro-positron emission tomography/computed tomography (μPET/CT) was used to monitor the tumor response in rats bearing orthotopic N1S1 hepatoma following transarterial injection of different embolic agents (Table 1). Compared with the nontreatment control, the PET signals of ^{18}F-FDG in the tumor sites disappeared 1 d after the rats were treated with Tyr-PVA-DEBs (TAE), I-DEBs with 0.2 mCi of ^{131}I (TARE^{low}), or D-DEBs with 0.5 mg of DOX (TACE^{low}) (Figure 5A). However, the ^{18}F-FDG signals in the tumor regions of these groups reappeared at late times postinjection, indicating tumor recurrence (Figure 5A, arrows). By contrast, the tumor-bearing rats did not exhibit recurrence during the entire monitoring period of 14 d following i.a. injection of I-DEBs with 0.5 mCi of ^{131}I (TARE^{hi}), D-DEBs with 2.5 mg of DOX (TACE^{hi}), or ID-DEBs with 0.2 mCi of ^{131}I plus 0.5 mg of DOX (TARCE$^{low/low}$). The results of maximum standard uptake values (SUV$_{max}$) of ^{18}F-FDG in the tumor revealed that TARCE$^{low/low}$ or TARE^{hi} induced the lowest SUV$_{max}$ among all the treatments at 14 d following the injection (Figure 5B). Histological analysis confirmed that the embolic microbeads remained in tumor blood vessels for at least 14 d (Figure S14). The tumor sizes and the results of H&E staining and Ki-67 immunofluorescence staining at 14 d confirmed tumor necrosis without significant tumor cell proliferation following TARE^{hi}, TACE^{hi}, or TARCE$^{low/low}$, consistent with the results of the ^{18}F-FDG μPET/CT imaging (Figure 5C and D). These data demonstrated that TARCE at low doses of ^{131}I and DOX produced an equivalent or higher antitumor effect in comparison with TARE at a high dose of ^{131}I or TACE at a high dose of DOX. The results of H&E staining further illustrated that TARCE$^{low/low}$ with ID-DEBs did not cause observed histological changes in major organs (Figure S15A). Comparatively, TACE^{hi} induced significant leisions in normal liver of the tumor-bearing rats at 14 d postinjection (Figure S15B, circled area), due to the high dose of DOX delivered. On the other hand, the administration doses of DOX and ^{131}I in TARCE$^{low/low}$ were one-fifth of TACE^{hi} and two-fifths of TARE^{hi}, respectively, effectively reducing the adverse effects. Collectively, TARCE with ID-DEBs generated a synergetic antitumor effect with a significant decrease of toxicity.

Table 1. Administration Doses of Different Treatment Groups of the Transarterial Embolization in Rats Bearing N1S1 Orthotopic Liver Cancer[a]

group	embolic agent	microbeads (mg)	DOX (mg)	^{131}I (mCi)
Control				
TAE	Tyr-PVA-DEBs	5		
TACE^{low}	D-DEBs	5	0.5	
TACE^{hi}	D-DEBs	5	2.5	
TARE^{low}	I-DEBs	5		0.2
TARE^{hi}	I-DEBs	5		0.5
TARCE$^{low/low}$	ID-DEBs	5	0.5	0.2

[a]Tyr-PVA-DEBs, tyrosine-substituted poly(vinyl alcohol) microbeads; D-DEBs, DOX-loaded Tyr-PVA-DEBs; I-DEBs, ^{131}I-labeled Tyr-PVA-DEBs; ID-DEBs, ^{131}I-DOX-loaded Tyr-PVA-DEBs; ^{low}, low dose; ^{hi}, high dose.

Synergetic Effect of DOX and ^{131}I to Overcome Resistance under Hypoxia. The above results of ^{18}F-FDG μPET/CT and histological analysis revealed that TARE or TACE at low doses inhibited the tumor proliferation but with recurrence. To investigate the underlying mechanism, we collected the tumor samples and found the upregulated expression of hypoxia-inducible factor 1-alpha (HIF-1α) throughout the tumor in the embolization groups at 3 d post-treatment (Figure 6A, green). This was because the embolic agents blocked the tumor blood vessels and cut off the oxygen supply to the tumor. Previous studies reported that upregulation of HIF-1α in the tumor was associated with poor prognosis and resistance to chemotherapy or radiotherapy.[33−35] Therefore, the extensive expression of HIF-1α as a result of the embolization-induced hypoxia could be the reason for the tumor recurrence.[33]

Compared with TARE^{low} or TACE^{low}, TARCE$^{low/low}$ induced higher levels of γ-H2AX expression in the tumor (Figures 6A, red, and S16A). This was in line with the more apoptotic cells observed in the TARCE$^{low/low}$-treated tumor (Figures 6B and S16B and C). These results confirmed that the hypoxia-induced resistance can be effectively alleviated by the combination therapy of ID-DEBs.

To prove this, we cultured N1S1 cells under hypoxia conditions. Compared to normoxia, hypoxia increased the IC$_{50}$ of DOX from D-DEBs by 4-fold (Figure 7A and B). The combined treatment with DOX and ^{131}I using ID-DEBs reversed the chemoresistance and reduced the IC$_{50}$ to 11.1% of that treated with DOX alone under hypoxia (D-DEBs/hypoxia). Similarly, hypoxia induced the radioresistance of the tumor cells, which was reversed by the combined treatment (Figure 7C and D). The CI of DOX and ^{131}I by ID-DEBs under hypoxia was calculated to be 0.23, much lower than the CI under normoxia (0.82), indicating a higher synergetic antitumor effect produced under hypoxia. The elevated expression of γ-H2AX in the cells treated with ID-DEBs further supported the sensitization of DOX to ^{131}I-induced DNA damage under hypoxia (Figure 7E).

https://dx.doi.org/10.1021/acsnano.0c09122
ACS Nano XXXX, XXX, XXX−XXX

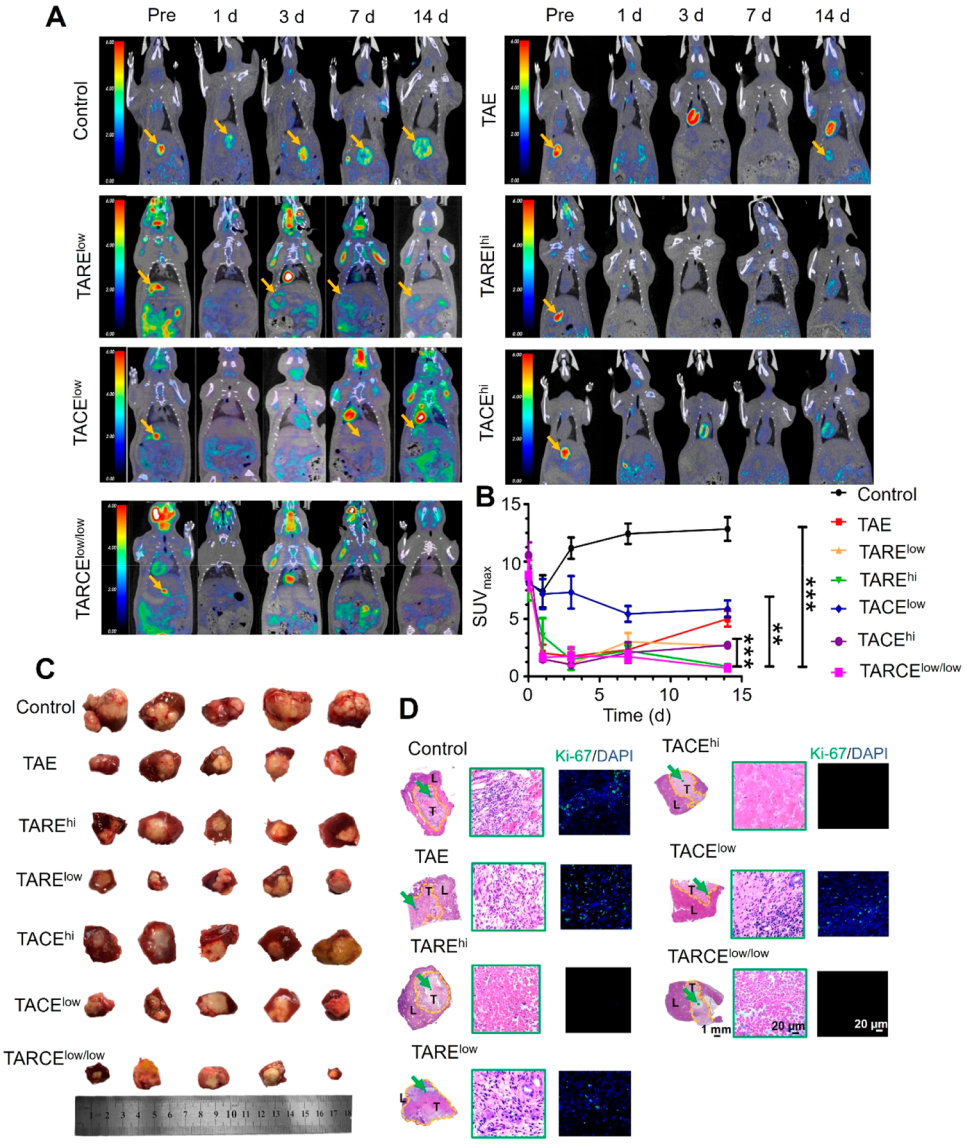

Figure 5. Enhanced antitumor effect following transarterial radio-chemoembolization (TARCE) with ID-DEBs at low dose. (A) Representative ^{18}F-FDG μPET/CT images of rats bearing orthotopic N1S1 tumor before (Pre) or at 1, 3, 7, or 14 d after i.a. injection of Tyr-PVA-DEBs (TAE), I-DEBs (TARE), D-DEBs (TACE), or ID-DEBs (TARCE). TARE^{hi} and TARE^{low}, I-DEBs with 0.5 and 0.2 mCi of ^{131}I, respectively. TACE^{hi} and TACE^{low}, D-DEBs with 2.5 and 0.5 mg of DOX, respectively. TARCE$^{low/low}$, ID-DEBs with 0.2 mCi of ^{131}I and 0.5 mg of DOX. Control, tumor-bearing rats without treatment. Yellow arrows, tumor. (B) Maximum standard uptake values (SUV$_{max}$) of ^{18}F-FDG by tumors in each group. Data are presented as mean ± SD (n = 5). **p < 0.01, ***p < 0.001 between the compared groups. Statistical significance was calculated by two-way ANOVA with Tukey's *post hoc* test. (C) Photographs of the resected tumors of each group at 14 d following the treatment (n = 5). (D) Representative micrographs of H&E staining and Ki-67 immunofluorescence in the tumor of each group. The tumor regions were separated from the normal liver tissues by yellow dotted lines. L, liver. T, tumor. Cell nuclei were stained with DAPI. Green arrows, the enlarged area.

CONCLUSIONS

In summary, we developed multifunctional PVA drug-eluting microbeads with high labeling stability of ^{131}I that offer tumor-specific radiotherapy as long as 31 d. The "permeant" embolization of ^{131}I-labeled PVA microbeads enables a tumor cumulative radiation dose of 345.04 ± 139.16 Gy by an injection dose as low as 0.2 mCi, resulting in 13 678-fold of that in normal tissues or higher. The significant advantage of the ^{131}I biodistribution profile by ^{131}I-labeled PVA microbeads proves the feasibility of ^{131}I-TARE at low dose and overcomes the limitations of ^{131}I-lipiodol. Besides, ^{131}I-labeled microbeads can be loaded with DOX and present a synergetic antitumor effect following TARCE through the sensitization of DOX to radiation-induced DNA damage under hypoxia by embolization. Our study demonstrates a combinatorial embolization therapy for hepatocellular carcinoma, *i.e.*, low dose-TARCE, and shows great potential for clinical translation.

MATERIALS AND METHODS

Materials. All the chemicals and reagents were purchased from Energy Chemical, Aladdin, Sigma-Aldrich Chemical, or Sinopharm Chemical unless otherwise specified and were used as received. Na^{131}I was ordered from XinKe Corporation (China).

Synthesis of NAAADA. NAAADA was synthesized according to previous reports with minor modifications.[36−38] Briefly, 400 mg of NaOH (10 mmol) was dissolved in ice-cold water, then mixed with 1.05 g of 2,2-dimethoxyethylamine (10 mmol). Acryloyl chloride (890

https://dx.doi.org/10.1021/acsnano.0c09122
ACS Nano XXXX, XXX, XXX−XXX

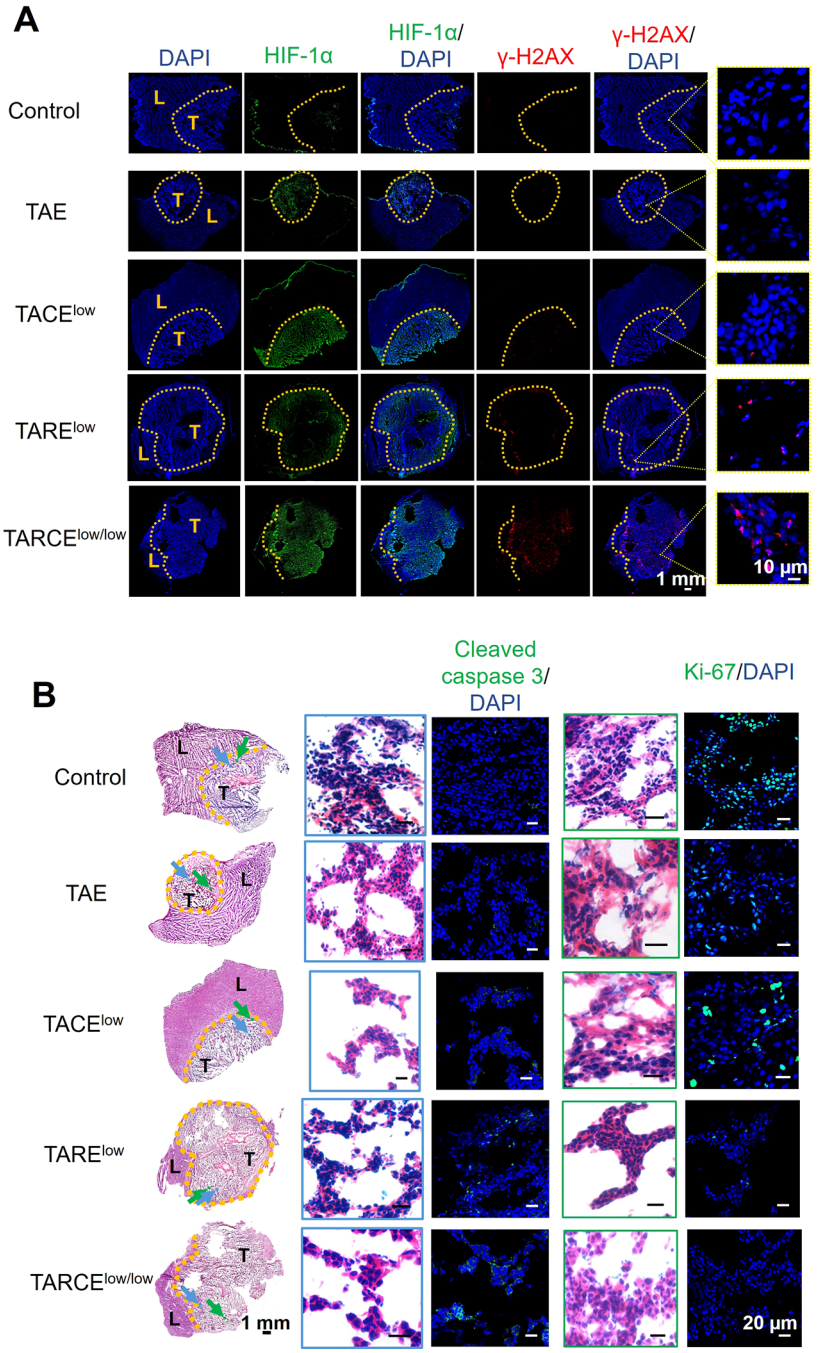

Figure 6. Enhanced antitumor effect of ID-DEBs under hypoxia induced by embolization. (A) Representative micrographs of immunofluorescence staining of HIF-1α and γ-H2AX in the tumor of each group at 3 d after the i.a. injection. (B) H&E staining and immunofluorescence staining of cleaved caspase 3 or Ki-67 of tumor from each group at 3 d after the i.a. injection. The tumor regions were separated from the normal liver tissues by yellow dotted lines. T, tumor. L, liver. Cell nuclei were counterstained with DAPI. The green and blue arrows in (B) indicate the enlarged area.

μL) was added to the mixture dropwise under stirring. The solution was stirred in ice-cold water for 3 h. The reaction mixture was saturated with sodium chloride and extracted three times with 15 mL of *tert*-butyl methyl ether. The organic phase was dried, filtered, and concentrated using a rotary evaporator. The resulting oil was extracted three times with petroleum ether and dried.

Synthesis of PVA-NAAADA. PVA-NAAADA was synthesized according to the previous report with minor modifications.[23] Briefly, 400 mg of the above synthesized NAAADA was added to 10 mL of 7.5% PVA-1799 solution dropwise under stirring. Then, 200 μL of concentrated hydrochloric acid was added to the solution and stirred at room temperature for 24 h. After the reaction, the pH of the solution was adjusted to 7 by adding a 2.5 M NaOH solution. The solid PVA-NAAADA was precipitated by adding an equal volume of acetone and washed twice with acetone, followed by overnight drying under vacuum.

Synthesis of NAT. NAT was synthesized according to previous reports with minor modifications.[39,40] Briefly, L-tyrosine (1.8 g, 10 mmol, Bidepharm, China) was dissolved in 8 mL of NaOH (3.25 M) aqueous solution. Acryloyl chloride (1.06 mL) was added to the solution dropwise under stirring. The solution was stirred in ice-cold water for 1 h followed by at room temperature for another 6 h. After the reaction, the pH of the solution was adjusted to 1−2 by adding concentrated hydrochloric acid. The reaction mixture was extracted

https://dx.doi.org/10.1021/acsnano.0c09122
ACS Nano XXXX, XXX, XXX−XXX

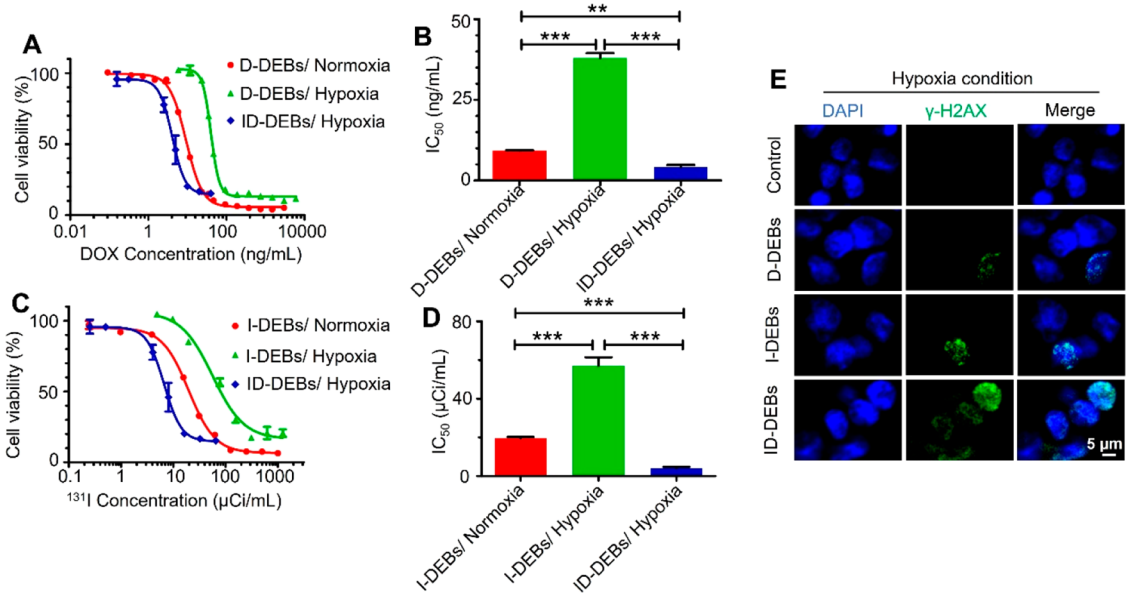

Figure 7. Synergetic antitumor cell effect of ^{131}I and DOX by ID-DEBs under hypoxia. (A) Viability of N1S1 cells treated with D-DEBs or ID-DEBs at various concentrations of DOX for 72 h determined by the MTT assay. (B) Comparison of IC_{50} values among the groups in (A). (C) Viability of N1S1 cells treated with I-DEBs or ID-DEBs at various concentrations of ^{131}I for 72 h determined by the MTT assay. (D) Comparison of IC_{50} values among the groups in (C). (E) Representative fluorescence micrographs of N1S1 cells following different treatments stained with anti-γ-H2AX. Cell nuclei were stained with DAPI. Data in (A)−(D) are represented as mean ± SD (n = 3). **p < 0.01, ***p < 0.001 between the compared groups in (B) or (D). Statistical significance was calculated by two-way ANOVA with Tukey's *post hoc* test.

three times with 20 mL of ethyl acetate. The organic phase was washed twice with 20 mL of 0.1 M HCl aqueous solution, then dried, filtered, and concentrated using a rotary evaporator to obtain a white, fluffy, solid product.

Preparation of Tyr-PVA-DEBs. Tyr-PVA-DEBs were prepared by inverse suspension polymerization according to a previously reported method for the preparation of AMPS-PVA-DEBs with modification.[23] Briefly, *N*-acryl tyrosine (120 mg) was dissolved in 120 μL of NaOH aqueous solution (400 mg/mL); then the pH of the solution was adjusted to 7 by adding concentrated hydrochloric acid. MBA (40 mg) and KPS (13 mg) were dissolved in 2 mL of 5% PVA-NAAADA solution, then mixed with NAT solution, as a water phase. Liquid paraffin (8 mL) containing 0.12 g of Span 80 was bubbled with N_2 for at least 15 min to remove O_2, as an oil phase. Under a N_2 flow, the water phase was added to the oil phase dropwise with stirring. After 10 min, 200 μL of a 10% TMEDA aqueous solution was added to the emulsion dropwise. The emulsion was kept in a 37 °C water bath for another 12 h under stirring in an inert atmosphere. After the reaction, the microspheres were separated by centrifugation at 4500 rpm for 5 min, then were sequentially washed with ethyl acetate, absolute alcohol, and water. The microspheres were further separated with mesh and dried under vacuum.

Characterization. ^{1}H NMR spectra were recorded on a Bruker AV400 at 400 MHz as $(CD_3)_2SO$ solutions with tetramethylsilane (δ = 0 ppm) as the internal standard. Fourier transform infrared (FT-IR) spectroscopy was performed on an FT-IR spectrometer (Equinox 55, Bruker) in the wavelength range between 4000 and 650 cm^{-1}. The morphologies of the microbeads and cross sections were observed by SEM (Ultra 55, Zeiss). The size distribution was measured by a Malvern Matersizer 3000. The images of the microbeads before and after drug loading were observed by an optical microscope.

For measurement of the particle number, 32.5 mg of Tyr-PVA-DEBs dry powder was weighed and suspended in 10 mL of ultrapure water. The number of particles in 5 mL of solution was measured by a particle counter (PST-890, Puluody), which was 65 845 particles. Each milligram of the microbeads was calculated to be 4052 particles. The maximum specific activity of I-DEBs was measured at about 1.7 mCi/mg. Therefore, the maximum radioactivity specific activity of each microsphere was calculated to be 15.5 kBq (1.7 mCi/mg × 37000 kBq/mCi ÷ 4052 particles/mg = 15.5 kBq/particle).

Drug Loading. Doxorubicin hydrochloride solutions (500 μL, Meilunbio, China) at different concentrations were added to 500 μL of the microbead solution (10 mg/mL) under stirring. Every 2 min, 10 μL of supernatant was withdrawn for analysis of DOX concentration using a UV−vis spectrophotometer (UV-2401PC, Shimadzu) at 483 nm. After the adsorption of DOX reached a stable state, the residual DOX in the supernatant was determined. The DOX distribution in the microbeads was investigated by confocal laser microscopy (LSM710, Zeiss). The drug-loading efficiency (DL) and encapsulation efficiency (EE) of the microspheres were calculated using the equations below.

$$\mathrm{DL\%} = \frac{m_{\mathrm{DOX}} - V_{\mathrm{supernatant}} \times C_{\mathrm{supernatant}}}{m_{\mathrm{DEBs}} + (m_{\mathrm{DOX}} - V_{\mathrm{supernatant}} \times C_{\mathrm{supernatant}})} \times 100\%$$

$$\mathrm{EE\%} = \frac{m_{\mathrm{DOX}} - V_{\mathrm{supernatant}} \times C_{\mathrm{supernatant}}}{m_{\mathrm{DOX}}} \times 100\%$$

where m_{DOX} and m_{DEBs} represent the mass of DOX and DEBs, respectively; $V_{supernatant}$ and $C_{supernatant}$ indicate the volume of the supernatant and the concentration of the residual DOX in the supernatant, respectively.

Release of DOX. The elution of DOX from the D-DEBs was measured using a previously reported method.[41] Briefly, 5 mg of D-DEBs was suspended in 8 mL of PBS (10 mM, pH7.4) at 37 °C in a shaking incubator at 150 rpm. Every 2 h, the concentration of doxorubicin was determined by withdrawing 3 mL of the release medium and replacing with an equal volume of fresh medium. For the DOX release study, D-DEBs were suspended in PBS (10 mM, pH 6.5 and 7.4) in the presence or absence of 10% FBS. Briefly, 5 mg of D-DEBs loading 0.5 mg of DOX was suspended in 10 mL of the release medium at 37 °C in a shaking incubator at 100 rpm. At predetermined time points, 1 mL aliquots were withdrawn and replaced with the same volume of the fresh medium.

^{131}I-Labeling. Tyr-PVA-DEBs were labeled with ^{131}I using the standard chloramine-T oxidation method.[42] Briefly, 5 mg of the

https://dx.doi.org/10.1021/acsnano.0c09122
ACS Nano XXXX, XXX, XXX−XXX

microbeads was suspended in 50 μL of 10 mM PBS and mixed with 50 μL of $Na^{131}I$ (0.3 or 1.0 mCi) solution and 10 μL of chloramine-T (100 mg/mL) solution. The mixture was incubated in 37 °C for 30 min. Free ^{131}I was removed by centrifugation completely and washed with water three times until there was no detachable gamma activity in the supernatant solution. The radiolabeling yield was measured by thin-layer chromatography (TLC, MiniScan, Eckert & Ziegler) using Whatman No. 1 filter paper and deionized water as a developing solvent. The labeled microbeads remained at the original spot, while free ^{131}I ions shifted to the strip front. The filter paper was cut into two halves, and each half was measured for radioactivity using a gamma counter (SN-697, Rihuan Instrument Factory). The stability of radiolabeled microbeads was analyzed by incubating I-DEBs or ID-DEBs with PBS (10 mM, pH 7.4) or 50% FBS at 37 °C. The radiolabeling yield was measured by TLC at the predetermined time points.

Cell Culture and Methyl Thiazolyl Tetrazolium (MTT) Assay. N1S1 cells (American Type Culture Collection, USA) were cultured in Iscove's modified Dulbecco's medium (IMDM) supplemented with 10% fetal bovine serum and 1% penicillin−streptomycin. The cells were incubated in a humidified atmosphere at 37 °C under normoxia (20% O_2/5% CO_2). The cells were seeded in 96-well plates at 5000 cells per well in 100 μL of IMDM medium and incubated overnight, followed by adding D-DEBs, I-DEBs, and ID-DEBs (100 μL in IMDM medium) at different concentrations, respectively. The cells were subjected to MTT assays after incubating for another 24, 48, and 72 h, respectively. The absorbance of the solution was measured on a microplate reader (Bio-Tek) at 560 and 690 nm. The relative cell viability was calculated (n = 3).

For the hypoxic treatment, N1S1 cells were placed in a sealed hypoxia chamber (UT208, Unitech Bioscience) equilibrated with certified gas containing 1% O_2, 5% CO_2, and 94% N_2.[43] For the viability test, N1S1 cells were preincubated for 72 h under hypoxia, then were seeded in 96-well plates at a density of 5000 cells per well in 100 μL of IMDM medium and incubated overnight, followed by being incubated with D-DEBs, I-DEBs, or ID-DEBs at different concentrations for another 72 h in hypoxia (n = 3).

The CI of DOX and ^{131}I was calculated using the equation below according to a previously reported method.[29]

$$CI = \frac{IC_{50DOX}}{IC_{50DOX'}} + \frac{IC_{50^{131}I}}{IC_{50^{131}I'}}$$

where $IC_{50DOX'}$ and $IC_{50^{131}I'}$ represent the IC_{50} values of DOX of D-DEBs and ^{131}I of I-DEBs, respectively. IC_{50DOX} and $IC_{50^{131}I}$ represent the IC_{50} values of DOX and ^{131}I of ID-DEBs, respectively.

Cell Cycle Analysis. The cell cycle analysis was performed according to a previously reported method.[44] Briefly, N1S1 cells were seeded in 12-well plates at a density of 3.5×10^5 cells per well in 1.5 mL of IMDM medium and incubated overnight. To the cultures were added 0.5 mL of IMDM medium as control, 400 μg/mL of D-DEBs in IMDM medium (157.2 ng/mL of DOX), 400 μg/mL of I-DEBs in IMDM medium (341.7 μCi/mL of ^{131}I), and 400 μg/mL of ID-DEBs in IMDM medium (157.2 ng/mL of DOX and 341.7 μCi/mL of ^{131}I), respectively. Each group was repeated three times and incubated for another 72 h. After the incubation, the cells were harvested and washed with PBS. The DEBs in the cell suspension were filtered out with a 40 μm nylon cell strainer. The cells were fixed with precooled 75% ethanol. After 30 min, the cells were washed with ice-cold PBS and stained with propidium iodide (50 μg/mL) for 30 min at 4 °C followed by flow cytometric analysis (CytoFLEX, Beckman Coulter). Data were analyzed with CytExpert software.

Comet Assay. After being treated with blank IMDM medium or IMDM medium with 400 μg/mL of D-DEBs (157.2 ng/mL of DOX), I-DEBs (341.7 μCi/mL of ^{131}I), or ID-DEBs (157.2 ng/mL of DOX and 341.7 μCi/mL of ^{131}I), the N1S1 cells were collected and washed with PBS. The Comet assay was carried out according to the manufacturer's protocols and the reported methods.[30,45] DNA was visualized by staining with 4′,6-diamidino-2-phenylindole (DAPI, Meilunbio, China) (10 μg/mL) and observed under a fluorescence microscope (DMI4000D, Leica). The degree of DNA damage was quantified by the ratio of comet tail (%), which was calculated through the Comet Assay Software Project (CASP).

Immunofluorescence Staining. After being treated with blank IMDM medium or IMDM medium with 400 μg/mL of D-DEBs (157.2 ng/mL of DOX), I-DEBs (341.7 μCi/mL of ^{131}I), or ID-DEBs (157.2 ng/mL of DOX and 341.7 μCi/mL of ^{131}I), the N1S1 cells were collected and washed with PBS, then fixed with ice-cold methanol for 15 min at −20 °C. The cells were washed with PBS and blocked with 5% FBS, followed by permeabilization with 0.3% Triton X-100 in PBS at room temperature for 20 min. After being washed with PBS, the cells were subsequently incubated with 100 μL of rabbit anti-rat γ-H2AX primary antibody (CST, 1:400) or rabbit anti-rat cleaved caspase 3 primary antibody (Boster, 1:100) at 4 °C overnight. After being washed with PBS, the cells were incubated with goat anti-rabbit Alexa Fluor 488 secondary antibody (Invitrogen, 1:500) for 1 h at room temperature, followed by DAPI-counterstaining. After being washed with PBS, the cells were added onto poly-L-lysine-coated microscopic slides. Then, the slides were mounted with Fluoromount-G (Southern Biotech) and examined under a confocal microscope (LSM710, Zeiss).

For the hypoxic study, N1S1 cells were preincubated for 72 h under hypoxia and treated with 0.5 mL of IMDM medium as control or IMDM medium with 400 μg/mL of D-DEBs (172.7 ng/mL of DOX), I-DEBs (280.7 μCi/mL of ^{131}I), or ID-DEBs (172.7 ng/mL of DOX and 280.7 μCi/mL of ^{131}I). Each group was treated for another 72 h and collected for immunofluorescence staining.

Western Blot Analysis. Western blot was performed according to a previously reported method.[46] The primary antibody was rabbit anti-γ-H2AX monoclonal antibody (CST, 1:1000), rabbit anti-cleaved caspase-3 monoclonal antibody (Boster, 1:500), rabbit anti-β-actin monoclonal antibody (CST, 1:1000), or mouse anti-GAPDH monoclonal antibody (Yeasen Biotech, 1:10 000). The second antibody was goat anti-rabbit HRP secondary antibody (Yeasen Biotech, 1:10 000) or goat anti-mouse HRP secondary antibody (Yeasen Biotech, 1:10 000).

Establishment of Tumor Model and Hepatic Artery Injection. All the animal procedures were in agreement with the guidelines of the Institutional Animal Care and Use Committee (IACUC) of Fudan University School of Pharmacy. Sprague−Dawley rats (male, 6−8 weeks) were purchased from Sino-British Sippr/BK Lab Animal Inc. For rats bearing the orthotopic N1S1 liver tumor model, the rats were anesthetized with an intraperitoneal injection of 40 mg/kg of pentobarbital. The abdomen skin of each rat was shaved. Following a 2 cm vertical midline cut, the left liver lobe was exposed for the injection of 40 μL of a PBS/matrigel mixture (v/v = 1:1) containing 7×10^6 N1S1 cells. The abdominal cavity was then sutured. ^{18}F-FDG μPET/CT scans were used to monitor the size of tumors after 7 d. The tumors of 8 ± 4 mm in diameter were used for the experiment at day 8. The hepatic artery injection was processed under a surgical microscope according to our previously reported procedure.[21]

μSPECT/CT Imaging and Internal Dosimetry Calculation. Three rats bearing orthotopic N1S1 liver tumors were injected with 5 mg of I-DEBs containing ∼0.2 mCi of ^{131}I through the hepatic artery and then imaged with a μSPECT/CT system (MILabs) at 1 h, 4 h, 1 d, 2 d, 3 d, 7 d, 14 d, 23 d, and 31 d postinjection, respectively. The imaging data were reconstructed using VivoQuant 4.0 software (Invicro). At 31 d, the rats were euthanized. Tumor, thyroid, normal liver, heart, spleen, lung, kidney, brain, muscle, bone, stomach, intestine, and bladder were excised and weighed, respectively. The radioactivity of each sample was measured by a gamma counter (GC1500, USTC Zonkia Scientific Instruments Co., Ltd.).

The volume of interest (VOI) of the standard tube and the signal area of the tumor site were delineated using PMOD software (version 4.0, PMOD Technologies), respectively. The curve of the radiation intensity of the tumor area with time was calculated by comparing the calibration tube. A VOI of a 5 mm diameter spherical signal area was delineated in the normal liver, thyroid, stomach, and muscle of the thigh, respectively. A curve of radioactivity per cubic centimeter of the

https://dx.doi.org/10.1021/acsnano.0c09122
ACS Nano XXXX, XXX, XXX−XXX

above tissues over time was plotted. The curve was fitted by an exponential function and integrated from 0 to infinity. The nuclide, VOI, and the area under the curve obtained after the integration were input into OLINDA software to calculate the cumulative radioactive dose per cubic centimeter of each organ, using the sphere as the simulation model.

Tumor Treatment. Eight days after the tumor cell inoculation, the tumor-bearing rats were randomly divided into 7 groups (n = 5). All the rats received hepatic artery injection. The embolic agents and the doses of each group are listed in Table 1. Control group rats did not receive treatment. The rats were imaged using a μPET/CT scanner at 1, 3, 7, or 14 d after ^{18}F-FDG (0.3 mL, 20 MBq, Renji Hospital, China) was injected into the tail vein. The uptake value was measured 30 min after the ^{18}F-FDG injection. Rats were maintained under anesthesia with 2% isoflurane during the acquisition.

Histological Analysis. Fifteen tumor-bearing rats were randomly divided into 5 groups (control group, TAE group, TACE^{low} group, TARE^{low} group, and TARCE$^{low/low}$ group, n = 3). At 3 d post-treatment, tumor tissues were collected for frozen sectioning and immunofluorescence staining. Primary antibody was mouse anti-rat HIF-1α antibody (Invitrogen, 1:500), rabbit anti-rat cleaved caspase-3 antibody (Boster, 1:100), rabbit anti-rat Ki-67 antibody (Invitrogen, 1:400), or rabbit anti-rat γ-H2AX antibody (CST, 1:400). The second antibody was goat anti-mouse Alexa Fluor 594 secondary antibody (Invitrogen, 1:500) or goat anti-rabbit Alexa Fluor 488 secondary antibody (Invitrogen, 1:500). The cell nuclei were counterstained with DAPI. The slices were mounted and observed by a Carl Zeiss LSM710 laser scanning microscope.

In a parallel experiment, at 14 d post-treatment, the rats were sacrificed. Half of the tumor tissues were frozen-sectioned for immunofluorescence staining of Ki-67 as described above. The other half were fixed with 4% paraformaldehyde for H&E staining.

Statistical Analysis. Statistical analysis was performed using GraphPad Prism 6 software (GraphPad). Data are presented as the mean ± SD for all results. Statistical significance was determined by one-way or two-way analysis of variance (ANOVA) with Tukey's multiple comparisons *post hoc* test.

ASSOCIATED CONTENT

Supporting Information

The Supporting Information is available free of charge at https://pubs.acs.org/doi/10.1021/acsnano.0c09122.

Additional experimental details including labeling lipiodol with ^{131}I for μSPECT/CT imaging, histological analysis of distribution of microbeads; supplemental Figures S1−S16 including characterization of NAAADA, PVA-NAAADA, NAT, DEBs, D-DEBs, and DOX-loaded AMPS-PVA-DEBs, radio thin-layer chromatogram of I-DEBs, procedure of hepatic artery injection, biodistribution of ^{131}I-lipiodol, H&E staining of tumor and liver with DEBs, cell viability of N1S1 tumor cells treated with D-DEBs or I-DEBs, histopathologic examination of the major organs of the tumor-bearing rats receiving different treatments, quantification of the immunofluorescence staining (PDF)

AUTHOR INFORMATION

Corresponding Authors

Wei Lu − *Minhang Hospital & School of Pharmacy, Key Laboratory of Smart Drug Delivery, Ministry of Education, & State Key Laboratory of Molecular Engineering of Polymers, Fudan University, Shanghai 201199, China*; orcid.org/0000-0002-1333-0274; Email: wlu@fudan.edu.cn

Shaoli Song − *Department of Nuclear Medicine, Fudan University Shanghai Cancer Center, Fudan University, Shanghai 200032, China*; Email: shaoli-song@163.com

Authors

Yuyi Qian − *Minhang Hospital & School of Pharmacy, Key Laboratory of Smart Drug Delivery, Ministry of Education, & State Key Laboratory of Molecular Engineering of Polymers, Fudan University, Shanghai 201199, China*

Qiufang Liu − *Department of Nuclear Medicine, Fudan University Shanghai Cancer Center, Fudan University, Shanghai 200032, China*

Panli Li − *Department of Nuclear Medicine, Fudan University Shanghai Cancer Center, Fudan University, Shanghai 200032, China*

Yaobao Han − *Center for Molecular Imaging and Nuclear Medicine, State Key Laboratory of Radiation Medicine and Protection, School for Radiological and Interdisciplinary Sciences (RAD-X), Soochow University, Suzhou 215123, China*

Jianping Zhang − *Department of Nuclear Medicine, Fudan University Shanghai Cancer Center, Fudan University, Shanghai 200032, China*

Jiaojiao Xu − *Minhang Hospital & School of Pharmacy, Key Laboratory of Smart Drug Delivery, Ministry of Education, & State Key Laboratory of Molecular Engineering of Polymers, Fudan University, Shanghai 201199, China*

Jingwen Sun − *Minhang Hospital & School of Pharmacy, Key Laboratory of Smart Drug Delivery, Ministry of Education, & State Key Laboratory of Molecular Engineering of Polymers, Fudan University, Shanghai 201199, China*

Aihua Wu − *Minhang Hospital & School of Pharmacy, Key Laboratory of Smart Drug Delivery, Ministry of Education, & State Key Laboratory of Molecular Engineering of Polymers, Fudan University, Shanghai 201199, China*

Complete contact information is available at: https://pubs.acs.org/10.1021/acsnano.0c09122

Author Contributions

$^{\perp}$Y.Q., Q.L., P.L., and Y.H. contributed equally to this work.

Notes

The authors declare the following competing financial interest(s): Y.Q. and W.L. submitted a patent application related to the findings in the manuscript.

ACKNOWLEDGMENTS

The authors thank J. Chen and T. Li from School of Pharmacy, Fudan University, for assisting in the experiment of μSPECT/CT imaging of the rats with ^{131}I-lipiodol. This work is supported in part by grants from the National Natural Science Foundation of China (91859110, 81991493, 81673018 to W.L. and 81771861 to S.S.), Program of Shanghai Academic Research Leader (19XD1420200 to W.L.), Shanghai Scientific and Technological Innovation Program (18410711200 to S.S.), and Shanghai Sailing Program (20YF1408400 to Q.L.).

REFERENCES

(1) Kim, H. C. Radioembolization for The Treatment of Hepatocellular Carcinoma. *Clin. Mol. Hepatol.* **2017**, *23*, 109−114.

(2) Sacco, R.; Conte, C.; Tumino, E.; Parisi, G.; Marceglia, S.; Metrangolo, S.; Eggenhoffner, R.; Bresci, G.; Cabibbo, G.; Giacomelli, L. Transarterial Radioembolization for Hepatocellular Carcinoma: a Review. *J. Hepatocell. Carcinoma.* **2016**, *3*, 25−29.

(3) Saini, A.; Wallace, A.; Alzubaidi, S.; Knuttinen, M. G.; Naidu, S.; Sheth, R.; Albadawi, H.; Oklu, R. History and Evolution of Yttrium-90 Radioembolization for Hepatocellular Carcinoma. *J. Clin. Med.* **2019**, *8*, 1−13.

(4) Tong, A. K.; Kao, Y. H.; Too, C. W.; Chin, K. F.; Ng, D. C.; Chow, P. K. Yttrium-90 Hepatic Radioembolization: Clinical Review and Current Techniques in Interventional Radiology and Personalized Dosimetry. *Br. J. Radiol.* **2016**, *89*, 20150943.
(5) Edeline, J.; Gilabert, M.; Garin, E.; Boucher, E.; Raoul, J. L. Yttrium-90 Microsphere Radioembolization for Hepatocellular Carcinoma. *Liver Cancer* **2015**, *4*, 16−25.
(6) Raoul, J. L.; Boucher, E.; Rolland, Y.; Garin, E. Treatment of Hepatocellular Carcinoma with Intra-Arterial Injection of Radionuclides. *Nat. Rev. Gastroenterol. Hepatol.* **2010**, *7*, 41−49.
(7) Van Der Gucht, A.; Jreige, M.; Denys, A.; Blanc-Durand, P.; Boubaker, A.; Pomoni, A.; Mitsakis, P.; Silva-Monteiro, M.; Gnesin, S.; Lalonde, M. N.; Duran, R.; Prior, J. O.; Schaefer, N. Resin *versus* Glass Microspheres for (90)Y Transarterial Radioembolization: Comparing Survival in Unresectable Hepatocellular Carcinoma Using Pretreatment Partition Model Dosimetry. *J. Nucl. Med.* **2017**, *58*, 1334−1340.
(8) Bouvry, C.; Palard, X.; Edeline, J.; Ardisson, V.; Loyer, P.; Garin, E.; Lepareur, N. Transarterial Radioembolization (TARE) Agents beyond (90)Y-Microspheres. *BioMed Res. Int.* **2018**, *2018*, 1−14.
(9) Raoul, J. L.; Bourguet, P.; Bretagne, J. F.; Duvauferrier, R.; Coornaert, S.; Darnault, P.; Ramee, A.; Herry, J. Y.; Gastard, J. Hepatic Artery Injection of I-131-Labeled Lipiodol. Part I. Biodistribution Study Results in Patients with Hepatocellular Carcinoma and Liver Metastases. *Radiology* **1988**, *168*, 541−545.
(10) Liapi, E.; Geschwind, J. F. Intra-Arterial Therapies for Hepatocellular Carcinoma: Where Do We Stand? *Ann. Surg. Oncol.* **2010**, *17*, 1234−1246.
(11) Jouneau, S.; Vauleon, E.; Caulet-Maugendre, S.; Polard, E.; Volatron, A. C.; Meunier, C.; Tattevin, P.; Montani, D.; Garin, E.; Raoul, J. L.; Delaval, P. 131I-Labeled Lipiodol-Induced Interstitial Pneumonia: a Series of 15 Cases. *Chest* **2011**, *139*, 1463−1469.
(12) Andreana, L.; Isgro, G.; Marelli, L.; Davies, N.; Yu, D.; Navalkissoor, S.; Burroughs, A. K. Treatment of Hepatocellular Carcinoma (HCC) by Intra-Arterial Infusion of Radio-Emitter Compounds: Trans-Arterial Radio-Embolisation of HCC. *Cancer Treat. Rev.* **2012**, *38*, 641−649.
(13) Thierens, H. M.; Monsieurs, M. A.; Bacher, K. Patient Dosimetry in Radionuclide Therapy: The Whys and The Wherefores. *Nucl. Med. Commun.* **2005**, *26*, 593−599.
(14) Kimura, T.; Aikata, H.; Doi, Y.; Imano, N.; Takeuchi, Y.; Takahashi, I.; Nishibuchi, I.; Katsuta, T.; Kenjo, M.; Murakami, Y.; Awai, K.; Chayama, K.; Nagata, Y. Comparison of Stereotactic Body Radiation Therapy Combined with or without Transcatheter Arterial Chemoembolization for Patients with Small Hepatocellular Carcinoma Ineligible for Resection or Ablation Therapies. *Int. J. Radiat. Oncol., Biol., Phys.* **2018**, *17*, 1−11.
(15) Jun, B. G.; Kim, S. G.; Kim, Y. D.; Cheon, G. J.; Han, K. H.; Yoo, J. J.; Kim, Y. S.; Jeong, S. W.; Jang, J. Y.; Lee, S. H.; Park, S.; Kim, H. S. Combined Therapy of Transarterial Chemoembolization and Stereotactic Body Radiation Therapy *versus* Transarterial Chemoembolization for ≤ 5 cm Hepatocellular Carcinoma: Propensity Score Matching Analysis. *PLoS One* **2018**, *13*, No. e0206381.
(16) Buckstein, M.; Kim, E.; Fischman, A.; Blacksburg, S.; Facciuto, M.; Schwartz, M.; Rosenzweig, K. Stereotactic Body Radiation Therapy Following Transarterial Chemoembolization for Unresectable Hepatocellular Carcinoma. *J. Gastrointest. Oncol.* **2018**, *9*, 734−740.
(17) Meng, M. B.; Cui, Y. L.; Lu, Y.; She, B.; Chen, Y.; Guan, Y. S.; Zhang, R. M. Transcatheter Arterial Chemoembolization in Combination with Radiotherapy for Unresectable Hepatocellular Carcinoma: a Systematic Review and Meta-analysis. *Radiother. Oncol.* **2009**, *92*, 184−194.
(18) Kim, S. W.; Oh, D.; Park, H. C.; Lim, D. H.; Shin, S. W.; Cho, S. K.; Gwak, G. Y.; Choi, M. S.; Paik, Y. H.; Paik, S. W. Transcatheter Arterial Chemoembolization and Radiation Therapy for Treatment-Naive Patients With Locally Advanced Hepatocellular Carcinoma. *Radiat. Oncol. J.* **2014**, *32*, 14−22.
(19) Lau, W. Y.; Lai, E. C.; Leung, T. W. Current Role of Selective Internal Irradiation with Yttrium-90 Microspheres in The Management of Hepatocellular Carcinoma: a Systematic Review. *Int. J. Radiat. Oncol., Biol., Phys.* **2011**, *81*, 460−467.
(20) Becker, S.; Laffont, S.; Vitry, F.; Rolland, Y.; Lecloirec, J.; Boucher, E.; Raoul, J. L.; Herry, J. Y.; Bourguet, P.; Garin, E. Dosimetric Evaluation and Therapeutic Response to Internal Radiation Therapy of Hepatocarcinomas Using Iodine-131-Labelled Lipiodol. *Nucl. Med. Commun.* **2008**, *29*, 815−825.
(21) Liu, Q.; Qian, Y.; Li, P.; Zhang, S.; Liu, J.; Sun, X.; Fulham, M.; Feng, D.; Huang, G.; Lu, W.; Song, S. 131I-Labeled Copper Sulfide-Loaded Microspheres to Treat Hepatic Tumors *via* Hepatic Artery Embolization. *Theranostics* **2018**, *8*, 785−799.
(22) Durante, A. C. R.; Sobra, D. V.; Miranda, A. C. C.; Almeida, E. V. D.; Fuscaldi, L. L.; Barboza, M. R. F. F. D.; Malavolta, L. Comparative Study of Two Oxidizing Agents, Chloramine T and Iodo-Gen®, for the Radiolabeling of *β*-CIT with Iodine-131: Relevance for Parkinson's Disease. *Pharmaceuticals* **2019**, *12*, 1−8.
(23) Ashrafi, K.; Tang, Y.; Britton, H.; Domenge, O.; Blino, D.; Bushby, A. J.; Shuturminska, K.; den Hartog, M.; Radaelli, A.; Negussie, A. H.; Mikhail, A. S.; Woods, D. L.; Krishnasamy, V.; Levy, E. B.; Wood, B. J.; Willis, S. L.; Dreher, M. R.; Lewis, A. L. Characterization of a Novel Intrinsically Radiopaque Drug-Eluting Bead for Image-Guided Therapy: DC Bead LUMI. *J. Controlled Release* **2017**, *250*, 36−47.
(24) Brown, K. T.; Do, R. K.; Gonen, M.; Covey, A. M.; Getrajdman, G. I.; Sofocleous, C. T.; Jarnagin, W. R.; D'Angelica, M. I.; Allen, P. J.; Erinjeri, J. P.; Brody, L. A.; O'Neill, G. P.; Johnson, K. N.; Garcia, A. R.; Beattie, C.; Zhao, B.; Solomon, S. B.; Schwartz, L. H.; DeMatteo, R.; Abou-Alfa, G. K. Randomized Trial of Hepatic Artery Embolization for Hepatocellular Carcinoma Using Doxorubicin-Eluting Microspheres Compared with Embolization with Microspheres Alone. *J. Clin. Oncol.* **2016**, *34*, 2046−2053.
(25) Yoon, W. Embolic Agents Used for Bronchial Artery Embolisation in Massive Haemoptysis. *Expert Opin. Pharmacother.* **2004**, *5*, 361−367.
(26) Chen, Y.; Song, G.; Dong, Z.; Yi, X.; Chao, Y.; Liang, C.; Yang, K.; Cheng, L.; Liu, Z. Drug-Loaded Mesoporous Tantalum Oxide Nanoparticles for Enhanced Synergetic Chemoradiotherapy with Reduced Systemic Toxicity. *Small* **2017**, *13*, 1−10.
(27) Zhong, X. Y.; Yang, K.; Dong, Z. L.; Yi, X.; Wang, Y.; Ge, C. C.; Zhao, Y. L.; Liu, Z. Polydopamine As a Biocompatible Multifunctional Nanocarrier for Combined Radioisotope Therapy and Chemotherapy of Cancer. *Adv. Funct. Mater.* **2015**, *25*, 7327−7336.
(28) Maiti, D.; Chao, Y.; Dong, Z.; Yi, X.; He, J.; Liu, Z.; Yang, K. Development of a Thermosensitive Protein Conjugated Nanogel for Enhanced Radio-Chemotherapy of Cancer. *Nanoscale* **2018**, *10*, 13976−13985.
(29) Lv, S.; Tang, Z.; Li, M.; Lin, J.; Song, W.; Liu, H.; Huang, Y.; Zhang, Y.; Chen, X. Co-delivery of Doxorubicin and Paclitaxel by PEG-Polypeptide Nanovehicle for the Treatment of Non-Small Cell Lung Cancer. *Biomaterials* **2014**, *35*, 6118−6129.
(30) Olive, P. L.; Banath, J. P. The Comet Assay: a Method to Measure DNA Damage in Individual Cells. *Nat. Protoc.* **2006**, *1*, 23−29.
(31) Tewey, K. M.; Rowe, T. C.; Yang, L.; Halligan, B. D.; Liu, L. F. Adriamycin-Induced DNA Damage Mediated by Mammalian DNA Topoisomerase II. *Science* **1984**, *226*, 466−468.
(32) Huang, P.; Zhang, Y.; Wang, W.; Zhou, J.; Sun, Y.; Liu, J.; Kong, D.; Liu, J.; Dong, A. Co-Delivery of Doxorubicin and 131I by Thermosensitive Micellar-Hydrogel for Enhanced *in Situ* Synergetic Chemoradiotherapy. *J. Controlled Release* **2015**, *220*, 456−464.
(33) Bowyer, C.; Lewis, A. L.; Lloyd, A. W.; Phillips, G. J.; Macfarlane, W. M. Hypoxia As a Target for Drug Combination Therapy of Liver Cancer. *Anti-Cancer Drugs* **2017**, *28*, 771−780.
(34) Dong, Z. Z.; Yao, M.; Wang, L.; Wu, W.; Gu, X.; Yao, D. F. Hypoxia-Inducible Factor-1alpha: Molecular-Targeted Therapy for Hepatocellular Carcinoma. *Mini-Rev. Med. Chem.* **2013**, *13*, 1295−1304.

https://dx.doi.org/10.1021/acsnano.0c09122
ACS Nano XXXX, XXX, XXX−XXX

(35) Xia, Y.; Jiang, L.; Zhong, T. The Role of HIF-1alpha in Chemo-/Radioresistant Tumors. *OncoTargets Ther.* **2018**, *11*, 3003−3011.
(36) Sivakumaran, D.; Mueller, E.; Hoare, T. Temperature-Induced Assembly of Monodisperse, Covalently Cross-Linked, and Degradable Poly(N-isopropylacrylamide) Microgels Based on Oligomeric Precursors. *Langmuir* **2015**, *31*, 5767−5778.
(37) Patenaude, M.; Campbell, S.; Kinio, D.; Hoare, T. Tuning Gelation Time and Morphology of Injectable Hydrogels Using Ketone-Hydrazide Cross-Linking. *Biomacromolecules* **2014**, *15*, 781−790.
(38) Smeets, N. M.; Bakaic, E.; Patenaude, M.; Hoare, T. Injectable and Tunable Poly(ethylene glycol) Analogue Hydrogels Based on Poly(oligoethylene glycol methacrylate). *Chem. Commun.* **2014**, *50*, 3306−3309.
(39) Harper, T.; Slegeris, R.; Pramudya, I.; Chung, H. Single-Phase Photo-Cross-Linkable Bioinspired Adhesive for Precise Control of Adhesion Strength. *ACS Appl. Mater. Interfaces* **2017**, *9*, 1830−1839.
(40) Chung, H.; Grubbs, R. H. Rapidly Cross-Linkable DOPA Containing Terpolymer Adhesives and PEG-Based Cross-Linkers for Biomedical Applications. *Macromolecules* **2012**, *45*, 9666−9673.
(41) Lewis, A. L.; Dreher, M. R.; O'Byrne, V.; Grey, D.; Caine, M.; Dunn, A.; Tang, Y.; Hall, B.; Fowers, K. D.; Johnson, C. G.; Sharma, K. V.; Wood, B. J. DC BeadM1: Towards an Optimal Transcatheter Hepatic Tumour Therapy. *J. Mater. Sci.: Mater. Med.* **2016**, *27*, 1−13.
(42) Yang, K.; Wan, J.; Zhang, S.; Zhang, Y.; Lee, S. T.; Liu, Z. *In Vivo* Pharmacokinetics, Long-Term Biodistribution, and Toxicology of PEGylated Graphene in Mice. *ACS Nano* **2011**, *5*, 516−522.
(43) Toh, Y. M.; Li, T. K. Mitoxantrone Inhibits HIF-1alpha Expression in a Topoisomerase II-Independent Pathway. *Clin. Cancer Res.* **2011**, *17*, 5026−5037.
(44) Chang, Y.; He, L.; Li, Z.; Zeng, L.; Song, Z.; Li, P.; Chan, L.; You, Y.; Yu, X. F.; Chu, P. K.; Chen, T. Designing Core-Shell Gold and Selenium Nanocomposites for Cancer Radiochemotherapy. *ACS Nano* **2017**, *11*, 4848−4858.
(45) Supiot, S.; Gouard, S.; Charrier, J.; Apostolidis, C.; Chatal, J. F.; Barbet, J.; Davodeau, F.; Cherel, M. Mechanisms of Cell Sensitization to Alpha Radioimmunotherapy by Doxorubicin or Paclitaxel in Multiple Myeloma Cell Lines. *Clin. Cancer Res.* **2005**, *11*, 7047s−7052s.
(46) Wang, X.; Guo, L.; Zhang, S.; Chen, Y.; Chen, Y. T.; Zheng, B.; Sun, J.; Qian, Y.; Chen, Y.; Yan, B.; Lu, W. Copper Sulfide Facilitates Hepatobiliary Clearance of Gold Nanoparticles through the Copper-Transporting ATPase ATP7B. *ACS Nano* **2019**, *13*, 5720−5730.

https://dx.doi.org/10.1021/acsnano.0c09122
ACS Nano XXXX, XXX, XXX−XXX